Investigating the Importance of the Flexible Hinge in Caerin 1.1: Solution Structures and Activity of Two Synthetically Modified Caerin Peptides†

Tara L. Pukala,‡ Craig S. Brinkworth,‡ John A. Carver,§ and John H. Bowie*,‡

Department of Chemistry, The University of Adelaide, Adelaide, South Australia 5005, Australia, and Department of Chemistry, University of Wollongong, Wollongong, New South Wales 2522, Australia

Received September 29, 2003; Revised Manuscript Received November 12, 2003

ABSTRACT: Caerin 1.1 is a potent broad-spectrum antibacterial peptide isolated from a number of Australian frogs of the *Litoria* genus. In membrane-like media, this peptide adopts two α-helices, separated by a flexible hinge region bounded by Pro15 and Pro19. Previous studies have suggested that the hinge region is important for effective orientation of the two helices within the bacterial cell membrane, resulting in lysis via the carpet mechanism. To evaluate the importance of the two Pro residues, they were replaced with either Ala or Gly. The antibacterial activity of these two peptides was tested, and their three-dimensional structures were determined using two-dimensional NMR spectroscopy and restrained molecular dynamics calculations. The resulting structures indicate that the central hinge angle decreases significantly upon replacement of the Pro residues with Gly and to a further extent with Ala. This trend was mirrored by a corresponding decrease in antibiotic activity, further exemplifying the necessity of the hinge in caerin 1.1 and related peptides. In a broader context, the use of Pro, Gly, and Ala variants of caerin 1.1 has enabled the relationship between conformational flexibility and activity to be directly investigated in a systematic manner.

The skin glands of amphibians contain a potent chemical arsenal, which forms an integral part of the animal's defense system and provides a means for regulation of dermal physiological function. Bioactive peptides exist as a significant component of this system, with more than 130 identified from the dermal secretion of over 25 species of Australian frogs investigated to date (*1*). In general, each frog possesses an assortment of active peptides, usually including a number of potent antibiotics with both broad and narrow spectrum components.

The caerin family forms the largest group of amphibian peptides discovered so far and, at present, comprises over 30 peptides isolated from the dermal secretions of six Australian frog species of the *Litoria* genus (*2*−*7*). These can be further divided into four groups, each of which contains a number of antimicrobially active compounds. All caerin 1 peptides have similar primary structures and are generally broad spectrum antibiotics particularly active against Gram-positive bacteria. Caerins 2−4, however, are commonly active only against a few of the species tested, typically *Escherichia coli* and *Micrococcus luteus*. The remaining inactive peptides are possibly the product of enzymic degradation. Table 1 presents sequences and antibacterial data for representative members of the caerin 1 family. Several additional members of this family have recently been identified by direct investigation of glandular genetic material (*8*).

Antibacterial amphibian peptides are generally short, α-helical species that act by disruption of bacterial cell membrane integrity. A number of mechanisms have been proposed to rationalize membrane penetration by the peptide, the simplest of which is the carpet mechanism (*9*−*11*). Interaction occurs at the membrane surface with the charged peptide attaching itself to ionic sites on the lipid bilayer (*1*). In this model, the peptides then enter the bilayer at an angle, as shown by FT-IR[1] (*12*) and solid-state NMR spectroscopy (*13*), and at a critical concentration cause strain on the bilayer and disruption of normal membrane function (*14*). Excessive flux of ions and small molecules across the cytoplasmic bilayer ultimately results in cell lysis. The solution structure of caerin 1.1 suggests that it forms two well-constructed amphipathic α-helices along the length of the peptide (between Leu2−Lys11 and Val17−His24), which are separated by a short central region of greater flexibility encompassing the proline residues at positions 15 and 19 (*15*). Proline residues are known to disrupt helical structure since they lack an amide proton and, as such, are unable to form the stabilizing hydrogen bonds to the carbonyl oxygen four residues previous. Since this motif is often a feature common to peptide antibiotics (*15*), the presence of central flexibility

† We thank the Australian Research Council for financial support of this project. C.S.B. acknowledges the award of an APRA Ph.D. scholarship.

* Address correspondence to this author. Tel: + 61 8 83035767. Fax: +61 8 83034358. E-mail: john.bowie@adelaide.edu.au.

‡ The University of Adelaide.

§ University of Wollongong.

[1] Abbreviations: ALLHDG, all hydrogen distance geometry; DQF-COSY, double-quantum-filtered correlation spectroscopy; FT-IR, Fourier transform infrared spectroscopy; HSQC, heteronuclear single-quantum coherence; MIC, minimum inhibitory concentration; NOESY, nuclear Overhauser effect spectroscopy; RMD, restrained molecular dynamics; SA, simulated annealing; TFE, trifluoroethanol; TOCSY, total correlation spectroscopy.

10.1021/bi035760b CCC: $27.50
Published on Web 01/03/2004

Table 1: Sequences and Antibacterial Activities of Selected Caerin 1 Peptides

name	sequence	name	sequence
caerin 1.1	GLLSVLGSVAKHVLPHVVPVIAEHL-NH_2	caerin 1.7	GLFKVLGSVAKHLLPHVAPVIAEKL-NH_2
caerin 1.2	GLLGVLGSVAKHVLPHVVPVIAEHL-NH_2	caerin 1.8	GLFKVLGSVAKHLLPHVVPVIAEKL-NH_2
caerin 1.3	GLLSVLGSVAQHVLPHVVPVIAEHL-NH_2	caerin 1.9	GLFGVLGSIAKHVLPHVVPVIAEKL-NH_2
caerin 1.4	GLLSSLSSVAKHVLPHVVPVIAEHL-NH_2	caerin 1.10	GLLSVLGDVAKHVLPHVVPVIAEKL-NH_2
caerin 1.5	GLLSVLGSVVKHVIPHVVPVIAEHL-NH_2	caerin 1.11	GLLGAMFKVASKVLPHVVPAITEHF−NH_2
caerin 1.6	GLFSVLGAVAKHVLPHVVPVIAEKL-NH_2		

	MIC[a] (μg/mL)										
organism	1.1	1.2	1.3	1.4	1.5	1.6	1.7	1.8	1.9	1.10	1.11
Bacillus cereus	50	50	50	50	50			50	50		
E. coli				50	100	50		100			
Leuconostoc lactis	1.5	25	25	12	3	3				6	6
Listeria innocua	25	100	100	100	50	50	20	25	25	50	
M. luteus	12		1.5	0.4	12	25	12	6	12	25	25
Pasteurella multocida	25		25	25	25	25	25	50	100	100	
Staphylococcus aureus	3−12		100	100	25	6−12	12−50	6−12	12		25−100
Staphylococcus epidermidis	12	50	100	25	25	12.5	50	12	25	100	50
Streptococcus uberis	12		100	100	50	25	50	25	25	50	100

[a] MIC is the minimum concentration required for pathogen growth inhibition (μg/mL). Where no figure is indicated, MIC is >100 μg/mL.

may be an important contributor to bioactivity, allowing the peptide to interact effectively with the cell membrane.

To further investigate the requirement of the hinge, structure−activity relationship studies can be performed in which critical proline residues are replaced. Glycine does possess an amide proton available for hydrogen bonding; however, its small side chain allows for increased conformational freedom compared with other residues. Thus, regions of greater flexibility occur in neighboring areas, particularly when multiple glycine residues are in close proximity (*16*). Conversely, alanine is considered a helix-promoting residue since it readily hydrogen bonds and has a larger side chain to restrict conformational rotation (*17*). Consequently, replacing both prolines of caerin 1.1 with either glycine (Gly15Gly19-caerin 1.1) or alanine (Ala15-Ala19-caerin 1.1) should give a series of peptides in which the effect of flexibility can be studied while maintaining other structural features such as charge and hydrophobicity. It is therefore anticipated that investigation of the structure and bioactivity of the modified caerin 1.1 analogues may confirm the helix-disrupting/helix-promoting nature assumed of proline, glycine, and alanine while providing further insight into the importance of the hinge region of caerin 1.1 and related antibacterial peptides.

EXPERIMENTAL PROCEDURES

Preparation of Synthetic Peptides. Peptides were synthesized by Mimotopes (Victoria, Australia) using L-amino acids and the standard *N*-α-Fmoc method. Full details, including protecting groups and deprotection, have been reported (*18*). Peptides were greater than 90% pure as determined by high-performance liquid chromatography and electrospray mass spectrometry.

Antibiotic Activity. Antibacterial testing was conducted by the Microbiology Department of the Institute of Medical and Veterinary Science (Adelaide, South Australia) and involved measurement of inhibition zones resulting from peptide application to microorganism-coated agarose plates (*19*). Activities are recorded as MIC values, which are the minimum concentrations (micrograms per milliliter) required to completely inhibit bacterial growth.

NMR Spectroscopy. The solution of Ala15Ala19-caerin 1.1 was prepared by dissolving the peptide (6.1 mg) in 95% TFE-d_3/5% H_2O (0.7 mL), giving a final concentration of 3.4 mM at a measured pH of 2.45. For Gly15Gly19-caerin 1.1, the peptide (5.0 mg) was dissolved in a mixture of H_2O (0.35 mL) and TFE-d_3 (0.35 mL), giving a final concentration of 2.9 mM at a measured pH of 3.50.

A Varian Inova-600 NMR spectrometer was used for acquisition of all NMR spectra, with a ^1H frequency of 600 MHz and a ^{13}C frequency of 150 MHz. Experiments were carried out at 25 °C and referenced to the methylene protons of residual unlabeled TFE (3.918 ppm). Referencing of the ^{13}C dimension of the HSQC spectrum was achieved using the $^{13}CH_2$ signal of TFE (60.975 ppm). Presaturation allowed for suppression of the water or residual TFE hydroxyl resonance in the TOCSY and NOESY experiments for Gly15Gly19-caerin 1.1 and was achieved by centering the transmitter frequency on this resonance and applying low-power presaturation from the proton transmitter during a 1.5 s relaxation delay between scans. WETNOESY and WET-TOCSY pulse sequences were employed for Ala15Ala19-caerin 1.1 to suppress the solvent resonance (*20*). Gradient methods for suppression were used in the DQF-COSY experiment in both cases (*21*). TOCSY, DQF-COSY, and NOESY experiments were collected in phase-sensitive mode, using time-proportional phase incrementation in t_1 (*22*). Typically, 32 time-averaged scans were acquired per increment, with a total of 256 increments for each experiment. The FID in t_2 consisted of 2048 data points over a spectral width of 6999.7 Hz (Ala15Ala19-caerin 1.1) or 5889.1 Hz (Gly15Gly19-caerin 1.1), and NOESY spectra were acquired with a mixing time of 150 or 125 ms, respectively. The HSQC experiment was recorded with an interpulse delay of $^1/_2J_{CH} = 3.6$ ms, corresponding to $J_{CH} = 140$ Hz. Again, 256 increments, each comprising 32 scans, were acquired over 4096 data points in the directly detected ^1H, F_2 dimension. A spectral width of 24132.7 Hz was used in the ^{13}C, F_1 dimension.

A Sun Microsystems Ultra Sparc 1/170 workstation and VNMR software (version 6.1A) were used to process the resulting spectra. The data matrices were multiplied by a

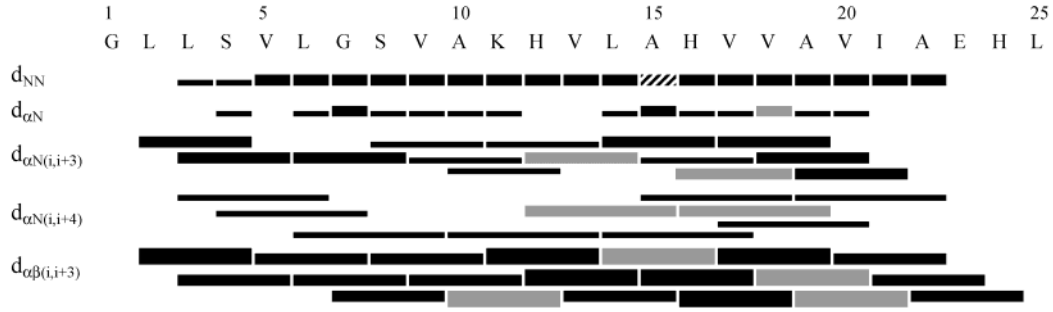

FIGURE 1: Summary of NOEs observed in the NOESY spectrum for Ala15Ala19-caerin 1.1 in TFE. The thickness of the bars indicates the relative strength of the signal (strong, <3.1 Å; medium, 3.1−3.7 Å; weak, >3.7 Å). Gray shaded boxes represent ambiguous NOEs, while the striped box represents signals too close to the diagonal for clear observation.

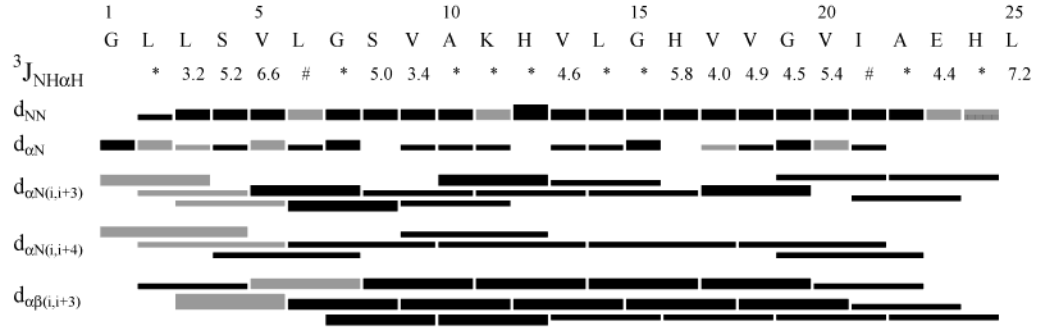

FIGURE 2: Summary of NOEs observed in the NOESY spectrum for Gly15Gly19-caerin 1.1 in TFE/H_2O (1:1 v/v). The thickness of the bars indicates the relative strength of the signal (strong, <3.1 Å; medium, 3.1−3.7 Å; weak, >3.7 Å). Gray shaded boxes represent ambiguous NOEs. $^3J_{NH\alpha H}$ values are indicated where possible. The pound sign (#) indicates the coupling constants, which could not be reliably assigned due to overlap, while the asterisk (*) indicates coupling constants that were not resolved.

Gaussian function in both dimensions before zero filling to 4096 data points prior to Fourier transformation. Final processed 2D NMR matrices consisted of 4096 × 4096 real points.

Structure Calculations. Sparky software (version 3.106) was used to assign ^{1}H resonances in the NOESY spectra via the sequential assignment procedure (*23*). For each symmetric pair of cross-peaks, the volume of the smaller peak was quantified and converted to distance restraints by the method of Xu et al. (*24*). $^3J_{NHC\alpha CH}$ values were measured from a 1D ^{1}H NMR spectrum acquired with 0.047 Hz per point digital resolution. Dihedral angles were restrained as follows: $^3J_{NHC\alpha CH} < 5$ Hz, $\phi = -60° \pm 30°$; 5 Hz $< {}^3J_{NHC\alpha CH} < 6$ Hz, $\phi = -60° \pm 40°$. For $^3J_{NHC\alpha CH}$ values ≥ 6, ϕ angles were not restrained.

Structures were generated using X-PLOR software (version 3.851) and a Sun Microsystems Sparc 1/170 workstation. The restrained molecular dynamics (RMD) and simulated annealing (SA) protocol was used (*25*), including the use of floating stereospecific assignments (*26*). Ambiguous restraints were managed by sum averaging and refined on the basis of structures resulting from preliminary calculations (*27*). Calculations were carried out using the all hydrogen distance geometry (ALLHDG) force field (version 4.03) (*28*). Sixty structures were generated initially with random backbone torsion angles and subjected to 6500 steps (19.5 ps) of high-temperature dynamics at 2000 K. The K_{NOE} and K_{repel} force constants were increased from 1000 to 5000 kcal·mol^{-1}·nm^{-2} and from 200 to 1000 kcal·mol^{-1}·nm^{-4}, respectively. Cooling to 1000 K followed in 2500 steps (7.5 ps), with K_{repel} increasing further to 40000 kcal·mol^{-1}·nm^{-4} and the atomic radii decreasing from 0.9 to 0.75 times those in the ALLHDG parameter set. Final cooling from 1000 to 100 K then occurred in 1000 steps (3 ps), and the resulting structures were subjected to 200 steps of conjugate gradient energy minimization. The 20 lowest potential energy structures produced were selected for analysis. Three-dimensional structures were viewed using INSIGHT II software (version 95.0, MSI) and the program MOLMOL (*29*).

RESULTS

NMR Studies. NMR spectra were acquired for Gly15Gly19-caerin 1.1 in aqueous TFE (1:1 v/v). Due to the poor solubility of Ala15Ala19-caerin 1.1 in this media, it was dissolved in 95% TFE, with 5% H_2O added to facilitate observation of NH proton resonances in the NMR spectra. ^{1}H chemical shifts were assigned using the sequential assignment procedure described by Wüthrich (*23*), while α-^{13}C resonances were assigned by investigation of ^{1}H−^{13}C HSQC spectra. A summary of all ^{1}H resonances and α-^{13}C chemical shifts for both Ala15Ala19-caerin 1.1 and Gly15-Gly19-caerin 1.1 is provided as Supporting Information.

Figures 1 and 2 display the diagnostic NOEs present in the NOESY spectra of both Ala15Ala19-caerin 1.1 and Gly15Gly19-caerin 1.1. In addition to the series of d_{NN} NOEs, a number of sequential $d_{\alpha N(i,i+1)}$ NOEs occur, as well as those from three and four residues apart ($d_{\alpha N(i,i+3)}$, $d_{\alpha\beta(i,i+3)}$, $d_{\alpha N(i,i+4)}$). The pattern of observed NOEs and their intensities is consistent with the peptides having helical structure along the majority of their sequence; however, the number of medium-range NOEs observed over the region of the hinge (residues 12−20) is greater for Ala15Ala19-caerin 1.1, suggesting that this peptide has more rigid α-helical structure

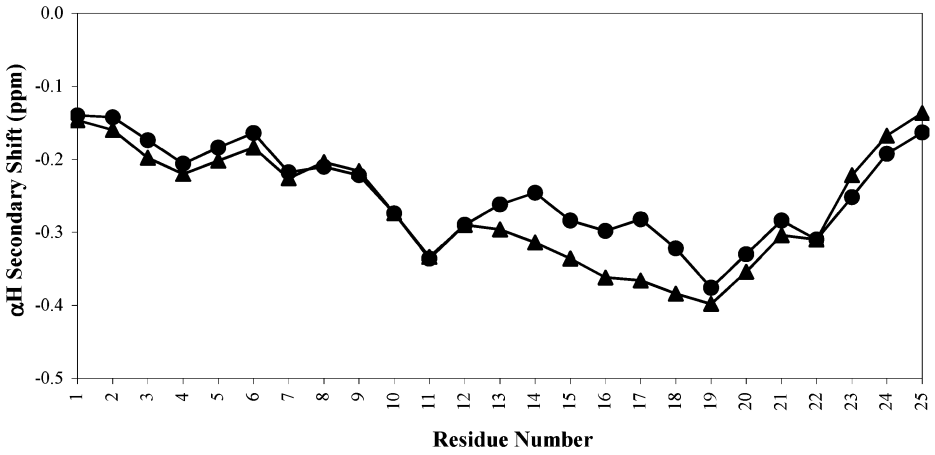

FIGURE 3: αH ^{1}H secondary shifts of (▲) Ala15Ala19-caerin 1.1 in TFE and (●) Gly15Gly19-caerin 1.1 in TFE/H_2O (1:1 v/v) smoothed over $n \pm 2$ residues. Negative values indicate an upfield shift from random coil resonances, while positive values indicate a shift downfield.

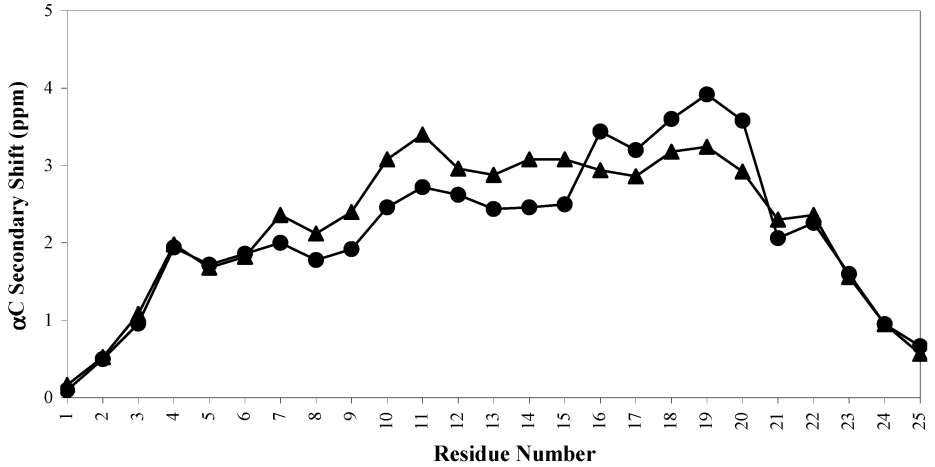

FIGURE 4: αC ^{13}C secondary shifts of (▲) Ala15Ala19-caerin 1.1 in TFE and (●) Gly15Gly19-caerin 1.1 in TFE/H_2O (1:1 v/v) smoothed over $n \pm 2$ residues. Negative values indicate an upfield shift from random coil resonances, while positive values indicate a shift downfield.

in comparison. No intermolecular NOEs were observed, implying the peptides are monomeric in solution.

The $^{3}J_{NH\alpha H}$ coupling constants (Figure 2), as determined from the NH region of the high-resolution 1D ^{1}H NMR spectrum, support the other observations that Gly15Gly19-caerin 1.1 adopts an α-helix between residues Leu3 and His24. Thus, in this region the majority of $^{3}J_{NH\alpha H}$ were ≤ 5 Hz, which implies helical structure. No $^{3}J_{NH\alpha H}$ coupling constants were resolvable for Ala15Ala19-caerin 1.1.

Random coil chemical shifts determined in water were obtained from the literature (*30*). The chemical shift differences between observed resonances and random coil values, $\Delta\delta$, were smoothed over a window of $n \pm 2$ residues and plotted against the amino acid sequence for αH and αC resonances (Figures 3 and 4) (*30*). NH secondary shifts were plotted as unsmoothed data (Figure 5).

Figure 3 demonstrates a distinct upfield shift from random coil values for αH resonances in both Ala15Ala19-caerin 1.1 and Gly15Gly19-caerin 1.1 along the majority of the peptide, while those for αC resonances are shifted downfield for both peptides (Figure 4). The magnitude and direction of secondary shift in both cases are consistent with the peptides having helical structure along their length (*31*). The difference in chemical shifts from random coil values is maximal throughout the center, while terminal regions approach random coil values. Flexibility at the ends of the peptide is anticipated however, due to the first and last four residues being less involved in the backbone hydrogen-bonding network responsible for helical structure (*32*). The secondary shifts (αH and αC) indicate slightly less helical character in the vicinity of Gly15 in the glycine analogue, since the magnitudes of the shifts in this region are considerably smaller than those of Ala15Ala19-caerin 1.1.

The magnitude of unsmoothed NH $\Delta\delta$ values deviates periodically over three to four residues for both Ala15Ala19-caerin 1.1 and Gly15Gly19-caerin 1.1, with hydrophobic residues generally producing resonances downfield compared with those which are hydrophilic (Figure 5). This pattern is again characteristic of an amphipathic α-helix and is due to differences in hydrogen bond lengths on either face of the peptide (*32*).

Structural Analysis. NOE intensities and dihedral angle restraints were used as input for structure calculations, which further supported the structural conclusions reached by inspection of NMR data. A total of 308 nonredundant restraints were produced for Ala15Ala19-caerin 1.1, of which 63 were sequential (i, $i + 1$), 47 were medium range (from two to four residues apart), and 53 were ambiguous. This compares with 67 sequential, 51 medium-range, and 32 ambiguous restraints in a total of 300 for Gly15Gly19-caerin 1.1. Eleven dihedral angle restraints were also employed for Gly15Gly19-caerin 1.1, based on observed $^{3}J_{NH\alpha H}$ coupling

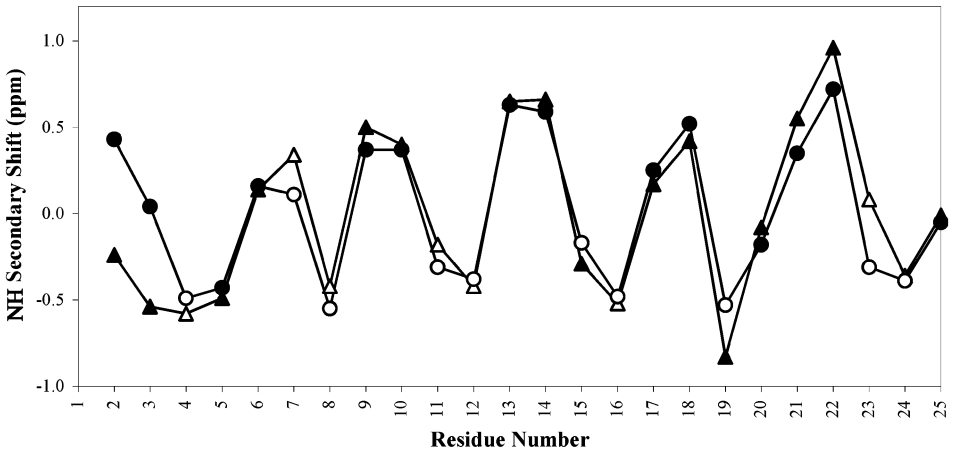

FIGURE 5: NH ^{1}H secondary shifts of (▲) Ala15Ala19-caerin 1.1 in TFE and (●) Gly15Gly19-caerin 1.1 in TFE/H_2O (1:1 v/v). Negative values indicate an upfield shift from random coil resonances, while positive values indicate a shift downfield. Hydrophilic residues are indicated by open symbols.

Table 2: Comparison of the Experimental Restraints Obtained from the NOESY Spectra of Ala15Ala19-caerin 1.1 and Gly15Gly19-caerin 1.1

no. of exptl restraints	Ala15Ala19-caerin 1.1	Gly15Gly19-caerin 1.1
sequential NOEs	63	67
medium-range NOEs	47	51
long-range NOEs	0	0
intraresidue NOEs	145	150
ambiguous NOEs	53	32
total	308	300

constants. The restraints used for each peptide are summarized in Table 2.

Sixty structures were generated for each peptide by the RMD and SA protocol, of which the 20 with lowest potential energy were chosen for analysis. Final structures demonstrate only minor deviation from idealized covalent geometry (≤0.05 Å for bonds, ≤5° for angles and impropers). A single restraint violation of 0.30 Å was observed for Ala15Ala19-caerin 1.1, while no restraint violations were observed for Gly15Gly19-caerin 1.1. The X-PLOR energy and structural statistics for both peptides are given in Table 3. The RMSD from mean geometry was substantially greater for Gly15Gly19-caerin 1.1, implying greater conformational freedom in this peptide. This can be further seen by overlaying the 20 lowest energy structures of each peptide from residues 2−15 (Figure 6). It is evident from this figure that the conformational range of the second helix is substantially greater for that of Gly15Gly19-caerin 1.1 in comparison with Ala15Ala19-caerin 1.1, again supporting the presence of greater structural variability about the glycine residues.

The most energetically stable of the 20 calculated structures for both Ala15Ala19-caerin 1.1 and Gly15Gly19-caerin 1.1 is shown in Figure 7, along with that of the native peptide for comparison (*15*, *33*). The extent of the hinge about Pro15 decreases significantly upon replacement with glycine and to a further extent with alanine. This in turn affects the amphipathicity of the molecule, with hydrophilic groups projecting into the hydrophobic face for both Ala15Ala19-caerin 1.1 and Gly15Gly19-caerin 1.1.

Angular order parameters (S, ϕ, and ψ) (*34*) of the final 20 structures were analyzed and indicated that a total of 19 residues (4−22) were well-defined ($S > 0.9$ for both ϕ and ψ) for Ala15Ala19-caerin 1.1. Similarly, all of the residues were well-defined for Gly15Gly19-caerin 1.1 with the exception of Gly1, Leu2, and Leu25. A Ramachandran plot (*35*) for average ϕ and ψ values of each peptide showed that all well-defined residues were distributed within the favored or allowed regions for α-helical structure (not shown).

DISCUSSION

Inspection of the solution structures of Ala15Ala19-caerin 1.1 and Gly15Gly19-caerin 1.1 reveals a significant difference in conformational freedom about the amino acid at position 15 between the two peptides, as exemplified by the hinge angle between the two helical regions that precede and follow residue 15 (Table 4). In addition, a direct comparison of the structural flexibility in this region of these peptides can be drawn from the RMSD values for residues about the hinge. These were 0.35 ± 0.13 and 0.66 ± 0.32 Å over the backbone atoms of residues 12−20 for Ala15Ala19-caerin 1.1 and Gly15Gly19-caerin 1.1, respectively, again supporting the extent of conformational variability over the ensemble of structures in each case. In turn, a correlation is observed between the magnitude of the hinge angle in the peptide and the antibacterial activity exhibited (Table 4). Caerin 1.1, the most active of the three peptides, has the largest hinge angle, while Ala15Ala19-caerin 1.1 with the smallest hinge angle is essentially inactive. Gly15Gly19-caerin 1.1 possesses a hinge angle between the other two peptides and exhibits intermediate bioactivity against the range of bacteria tested.

The polarity of alanine, glycine, and proline is comparable, so variation in this property is unlikely to contribute significantly to the differences observed in the bioactivity of caerin 1.1 and these two analogues. Alanine and glycine exhibit both hydrophobic and hydrophilic characteristics. Hence, in the context of amphipathic membrane-active helices, interchanging these residues should not adversely affect interaction of the resultant peptide with the membrane (*36*, *37*). Other factors known to impact on the activity of membrane-active peptides include helicity and amphipathicity (*15*, *38*) and, consequently, form the basis of this structure−activity relationship. As demonstrated by Wong et al. (*15*), placing the complete amino acid sequence of caerin 1.1 on a Schiffer−Edmundson wheel projection

Table 3: Structural Statistics of Ala15Ala19-caerin 1.1 and Gly15Gly19-caerin 1.1 following RMD/SA Calculations

	Ala15Ala19-caerin 1.1		Gly15Gly19-caerin 1.1	
	⟨SA⟩[a]	$(SA)_r$[b]	⟨SA⟩	$(SA)_r$
well-defined residues	4−22		3−24	
X-PLOR energies (kcal·mol^{-1})				
E_{tot}	40.30 ± 7.12	24.26	27.39 ± 7.29	8.77
E_{bond}	1.83 ± 0.48	1.09	1.10 ± 0.36	0.14
E_{angle}	19.42 ± 3.91	11.24	13.17 ± 2.75	7.04
$E_{improper}$	4.01 ± 1.21	1.33	1.09 ± 0.67	0.17
E_{vdW}	5.37 ± 1.05	4.19	4.97 ± 2.54	0.11
E_{NOE}	9.67 ± 2.92	6.41	7.07 ± 2.41	1.31
E_{cdih}	0.00	0.00	0.00	0.00
RMSD from mean geometry (Å)				
backbone atoms of well-defined residues	0.62 ± 0.22		1.28 ± 0.53	
all backbone atoms	1.26 ± 0.38		1.58 ± 0.64	
heavy atoms of well-defined residues	0.87 ± 0.20		1.77 ± 0.61	
all heavy atoms	1.60 ± 0.41		1.97 ± 0.65	

[a] ⟨SA⟩ is the collection of 20 final structures. [b] (SA) is the mean structure obtained by best-fitting and averaging the coordinates of the backbone atoms in the final 20 structures, and $(SA)_r$ is the representative structure after energy minimization of (SA).

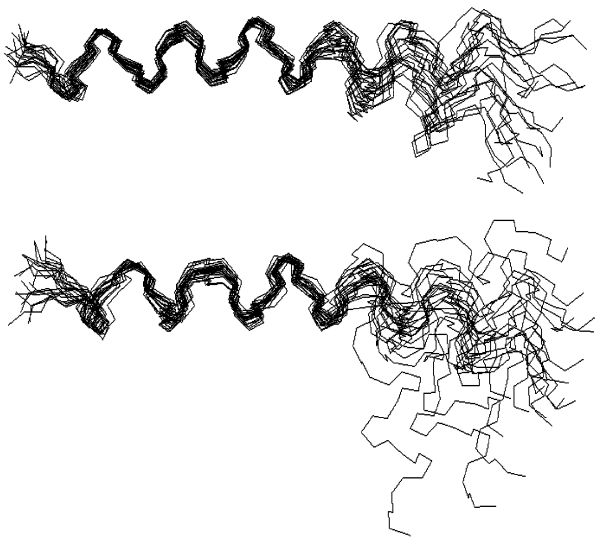

FIGURE 6: The 20 most stable calculated structures of Ala15Ala19-caerin 1.1 (top) and Gly15Gly19-caerin 1.1 (bottom) superimposed along the backbone atoms (N, αC, and carbonyl C) of residues 2−15.

reveals that the peptide does not conform to an amphipathic helical structure along its entire length. However, by separately plotting the residues before and after Pro15, it becomes apparent that the peptide can adopt an amphipathic α-helical conformation from Gly1 to Leu14 and from His16 to Leu25, with the center of the latter helix being shifted in orientation by approximately 140° compared with the former (*15*). Therefore, the observed flexibility in the central region of caerin 1.1 could enable reorientation of the two helices, resulting in an overall amphipathic molecule. This is supported by the solution structure of this peptide (Figure 7), in which the two α-helices are oriented such that their side chains form a continuous hydrophobic face on the concave side of the peptide and a hydrophilic face on the convex side.

Solid-state NMR studies have shown that caerin 1.1 acts via the carpet mechanism, in which the N-terminal amphipathic helix interacts with the solvent-exposed face of the membrane via its basic residues, while the C-terminal α-helix is inserted into the bilayer (*13*). Amphipathicity is important in this model since it allows the hydrophilic face to maintain contact with polar groups and water phases, while the hydrophobic face can interact with lipid acyl side chains and effect permeation. As the hinge angle decreases along with conformational flexibility in the central region about Pro15, so does the ability of the peptide to reorient the two helices. As such, the formation of an amphipathic structure is not facilitated in these species. Thus, the rigidity imparted by the two alanine residues in Ala15Ala19-caerin 1.1 leads to an almost ideal α-helix along its length. As a consequence, there is no clear hydrophobic face in Ala15Ala19-caerin 1.1, with the hydrophilic residues, Ser4 and Lys11, projecting into the hydrophobic region (Figure 7). In Gly15Gly19-caerin 1.1, Lys11 is oriented at the interface of the two regions, but all other residues line up on their expected face depending on their polarity.

Electrostatic interactions between the peptide and the membrane are the driving force of the carpet mechanism. Consequently, the position of the side chain of Lys11 in Ala15Ala19-caerin 1.1 would prohibit its interaction with the negatively charged membrane, thus affecting the ability of the peptide to bind to the bilayer surface. The reduction in membrane affinity in turn reduces the likelihood of reaching the critical concentration required for permeability. In contrast, the side chain of Lys11 in Gly15Gly19-caerin 1.1 is still in an orientation that is capable of interacting with the hydrophilic surface of the membrane and thereby assisting in binding. However, as a result of the reduced hinge angle and central flexibility, its C-terminal helix is not able to protrude as deeply into the bilayer, which may account for the reduced antibiotic activity of this peptide.

The solution structures of a number of antimicrobial peptides have been shown to adopt a dual amphipathic helical arrangement with central flexibility [e.g., cecropin A (*39*), sarcotoxin IA (*40*), and buforin II (*41*)], demonstrating the importance of this structural feature for activity. In addition, maculatin 1.1 has been isolated from the skin secretion of *Litoria genimaculata* and shares significant sequence similarity with caerin 1.1, differing only by the absence of four central residues (His12−Pro15 of caerin 1.1) (*42*). This peptide shows a comparable spectrum of antibiotic activity to caerin 1.1, and its NMR-derived solution structure is also similar, adopting a helical structure with a hinge about Pro15 (*17*). As for caerin 1.1, changing Pro15 in maculatin 1.1 to

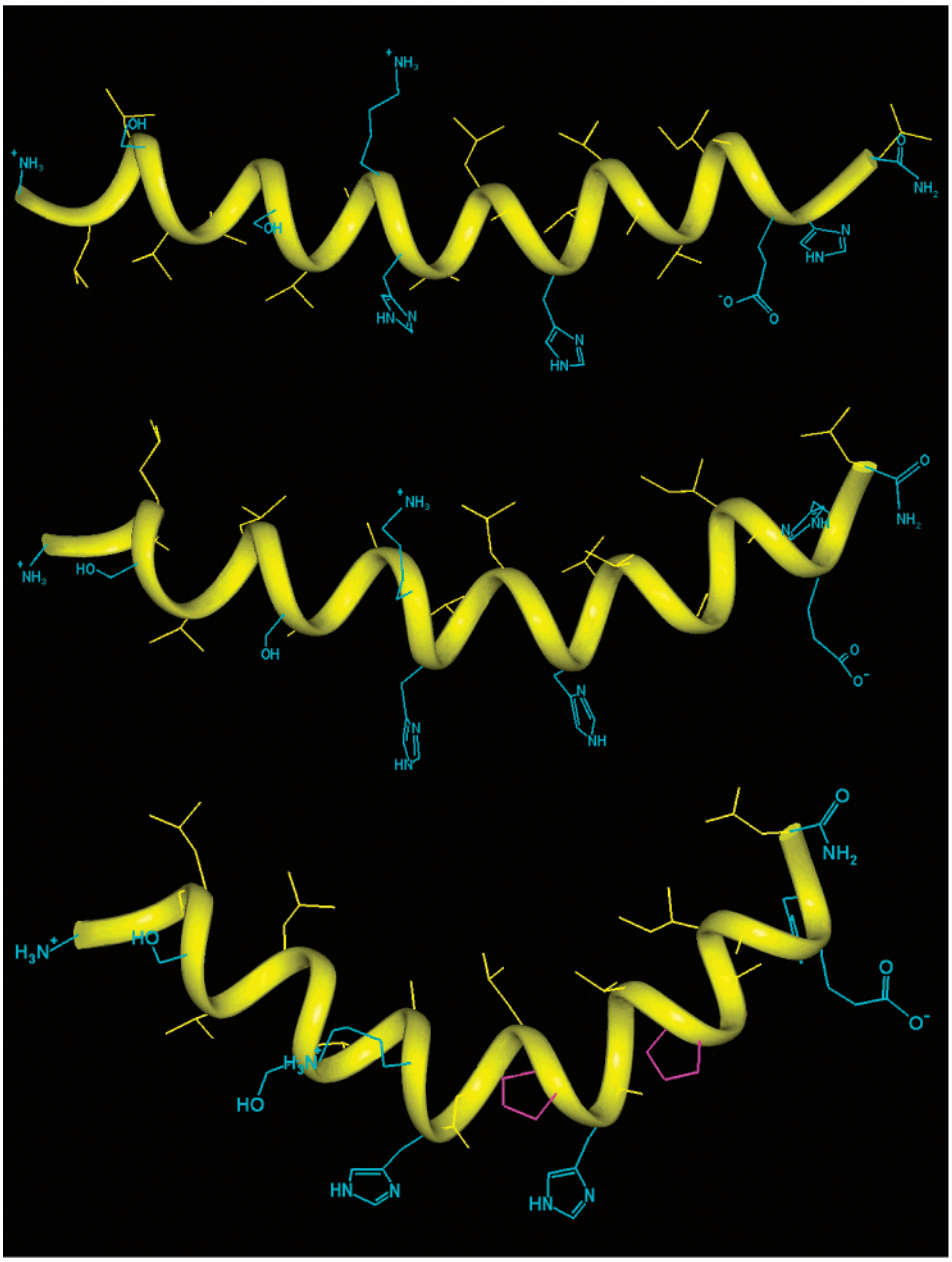

FIGURE 7: The most stable calculated solution structures of caerin 1.1 (bottom), Gly15Gly19-caerin 1.1 (middle), and Ala15Ala19-caerin 1.1 (top). Hydrophilic groups are colored blue, while hydrophobic groups are in yellow. Proline residues are indicated in pink.

an alanine reduces the bioactivity of the peptide 5−10-fold against a range of bacteria (*17*). Structurally, like caerin 1.1, this is a result of alanine promoting formation of a linear helix, thereby hindering reorientation of the two helices and reducing amphipathicity in the molecule (*17*).

In contrast to the aforementioned peptides which are thought to act via a carpet-like mechanism, there are a number of proline-hinge-containing peptides which cause cell lysis via formation of transmembrane pores. The most widely studied example is melittin, a 26 amino acid peptide from bee venom, which lyses cell membranes and induces voltage-dependent ion conductance in lipid bilayers (*43*−*45*). Substituting Pro14 in melittin with alanine gives a peptide which lacks the flexibility normally imparted by the central proline residue (*46*, *47*). Interestingly, in experiments with human erythrocytes, Ala14-melittin caused biphasic hemolysis kinetics similar to that of the native peptide but was much more efficient at lysis (*47*). However, Ala14-melittin was not as good as melittin in inducing voltage-dependent ion conductance (*47*). Thus, alanine substitution in melittin reduced the ion-channel-forming propensity of the peptide but enhanced its lytic ability; i.e., the two properties are not coupled (*47*). The reasons for this apparent dichotomy are not clear, but they may imply that Pro14-melittin does not elicit its lytic activity exclusively via pore formation. The significant variation in the effects of central proline substitution on melittin and caerin 1.1 function implies major differences in the requirements of the pore and the carpet mechanisms of membrane disruption.

CONCLUSION

Ala15Ala19-caerin 1.1 forms a well-defined helix along its entire length with the loss of the flexible hinge region for Ala15Ala19-caerin 1.1 compared with the natural peptide, confirming the helix-disrupting nature of proline. The Gly15Gly19-caerin peptide has flexibility that is intermediate

Table 4: Correlation between Hinge Angle and Antibiotic Activity in Caerin 1.1, Gly15Gly19-caerin 1.1, and Ala15Ala19-caerin 1.1

	peptide		
	caerin 1.1	Gly15Gly19-caerin 1.1	Ala15Ala19-caerin 1.1
hinge angle[a] (deg)	75	40	15
MIC[b] (μg/mL)			
B. cereus	50	50	
E. coli		50	
L. lactis	1.5	12	50
L. innocua	25	50	
M. luteus	12	12	
P. multocida	25	100	
S. aureus	3−12	25−50	
S. epidermidis	12	100	
S. uberis	12	12	

[a]The hinge angle is defined as the angle between the C- and N-terminal helices in the lowest energy structure. [b] MIC is the minimum concentration required for pathogen growth inhibition (μg/mL). Where no figure is indicated, MIC is >100 μg/mL.

between these two other peptides. These data support the initial assumptions made regarding the helix-promoting or helix-disrupting nature of alanine, glycine, and proline. Reduction in central flexibility observed throughout this series of peptides is mirrored by a decrease in biological activity, suggesting a direct relationship between these factors. It is likely that the flexible hinge about Pro15 allows optimal orientation of both the C- and N-terminal amphipathic α-helices of caerin 1.1 within the membrane. Consequently, an absence of this property may be responsible for the peptide no longer interacting effectively with bacterial cell membranes, decreasing the binding and permeabilizing ability of these peptides. This would in turn account for the significant decrease in biological efficacy observed.

SUPPORTING INFORMATION AVAILABLE

A summary of all ^{1}H resonances and α-^{13}C chemical shifts for Ala15Ala19-caerin 1.1 and Gly15Gly19-caerin 1.1. This material is available free of charge via the Internet at http://pubs.acs.org.

REFERENCES

1. Bowie, J. H., Wegener, K. L., Chia, B. C. S., Wabnitz, P. A., Carver, J. A., Tyler, M. J., and Wallace, J. C. (1999) *Protein Pept. Lett. 6*, 259−269.
2. Stone, D. J. M., Waugh, R. J., Bowie, J. H., Wallace, J. C., and Tyler, M. J. (1992) *J. Chem. Soc., Perkin Trans. 1*, 3173−3178.
3. Waugh, R. J., Stone, D. J. M., Bowie, J. H., Wallace, J. C., and Tyler, M. J. (1993) *J. Chem. Res. (S) 139* (M), 937−961.
4. Waugh, R. J., Stone, D. J. M., Bowie, J. H., Wallace, J. C., and Tyler, M. J. (1993) *J. Chem. Soc., Perkin Trans. 1*, 573−576.
5. Steinborner, S. T., Waugh, R. J., Bowie, J. H., and Tyler, M. J. (1997) *Rapid Commun. Mass Spectrom. 11*, 997−1000.
6. Steinborner, S. T., Bowie, J. H., Tyler, M. J., and Wallace, J. C. (1997) *Aust. J. Chem. 50*, 889−894.
7. Steinborner, S. T., Currie, G. J., Bowie, J. H., Wallace, J. C., and Tyler, M. J. (1998) *J. Pept. Res. 51*, 121−126.
8. Vanhoye, D., Brustion, F., Nicolas, P., and Amiche, M. (2003) *Eur. J. Biochem. 270*, 2068−2081.
9. Shai, Y. (1999) *Biochim. Biophys. Acta 1462*, 55−70.
10. Bechinger, B. (1999) *Biochim. Biophys. Acta 1462*, 157−183.
11. Oren, Z., and Shai, Y. (1998) *Biopolymers 47*, 451−463.
12. Chia, B. C. S., Torres, J., Cooper, M. A., Arkin, I. T., and Bowie, J. H. (2002) *FEBS Lett. 512*, 47−51.
13. Marcotte, I., Wegener, K. L., Lam, Y. H., Chia, B. C. S., de Planque, M. R. R., Bowie, J. H., Auger, M., and Separovic, F. (2003) *Chem. Phys. Lipids 122*, 107−120.
14. Epand, R. M., Shai, Y. C., Segrest, J. P., and Anantharamaiah, G. M. (1995) *Biopolymers 37*, 319−338.
15. Wong, H., Bowie, J. H., and Carver, J. A. (1997) *Eur. J. Biochem. 247*, 545−557.
16. Oh, D., Shin, S. Y., Lee, S., Kang, J. H., Kim, S. D., Ryu, P. D., Hahm, K., and Kim, Y. (2000) *Biochemistry 39*, 11855−11864.
17. Chia, B. C. S., Carver, J. A., Mulhern, T. D., and Bowie, J. H. (2000) *Eur. J. Biochem. 267*, 1894−1908.
18. Maeji, N. J., Bray, A. M., Valerio, R. M., and Wang, W. (1995) *Pept. Res. 8*, 33−38.
19. Jorgensen, J. H., Cleeland, W. A., Craig, G., Doern, M., Ferraro, J., Finegold, C. M., Hansen, S. L., Jenkins, S. G., Novick, W. J., Pfaller, M. S., Preston, D. A., Reller, L. B., and Swanson, J. M. (1993) *Natl. Comm. Clin. Lab. Stand. 33*, 1−12.
20. Smallcombe, S. H., Patt, S. L., and Kiefer, P. A. (1995) *J. Magn. Reson. 117*, 295−303.
21. John, B. K., Plant, D., Webb, P., and Hurd, R. E. (1992) *J. Magn. Reson. 98*, 200−206.
22. Marion, D., and Wüthrich, K. (1983) *Biochem. Biophys. Res. Commun. 113*, 967−974.
23. Wüthrich, K. (1986) *NMR of Proteins and Nucleic Acids*, John Wiley & Sons, New York.
24. Xu, R. X., Word, J. M., Davis, D. G., Rink, M. J., Willard, D. H., and Gampe, R. T. (1995) *Biochemistry 34*, 2107−2121.
25. Nilges, M., and O'Donoghue, S. I. (1998) *Prog. Nucl. Magn. Reson. Spectrosc. 32*, 107−139.
26. Folmer, R. H. A., Hilbers, C. W., Konings, R. N. H., and Nilges, M. (1997) *J. Biomol. NMR 9*, 245−258.
27. Weber, P. L., Morrison, R., and Hare, D. (1988) *J. Mol. Biol. 204*, 483−487.
28. Engh, R. A., and Huber, R. (1991) *Acta Crystallogr. A47*, 392−400.
29. Koradi, R., Billeter, M., and Wüthrich, K. (1996) *J. Mol. Graphics 14*.
30. Wishart, D. S., Bigam, C. G., Holm, A., Hodges, R. S., and Sykes, B. D. (1995) *J. Biomol. NMR 5*, 67−81.
31. Wishart, D. S., Sykes, B. D., and Richards, F. M. (1991) *J. Mol. Biol. 222*, 311−333.
32. Zhou, N. E., Zhu, B., Sykes, B. D., and Hodges, R. S. (1992) *J. Am. Chem. Soc. 114*, 4320−4326.
33. Wegener, K. L., Carver, J. A., and Bowie, J. H. (2003) *Biopolymers 69*, 42−59.
34. Pallaghy, P. K., Duggan, B. M., Pennington, M. W., and Norton, R. S. (1993) *J. Mol. Biol. 234*, 405−420.
35. Morris, A. L., MacArthur, M. W., Hutchinson, E. G., and Thornton, J. M. (1992) *Proteins: Struct., Funct., Genet. 12*, 345−364.
36. Bechinger, B. (2001) *Biophys. J. 81*, 2251−2256.
37. Sanan-Mishra, A. N., Tuteja, N., and Sopory, S. K. (2002) *Biochem. Biophys. Res. Commun. 269*, 1063−1068.
38. Subbalakshmi, C., Nagaraj, R., and Sitaram, N. (1999) *FEBS Lett. 448*, 62−66.
39. Holak, T. A., Engstrom, A., Kraulis, P. J., Lindeberg, G., Bennich, H., Jones, T. A., Gronenborn, A. M., and Clore, G. M. (1988) *Biochemistry 27*, 7620−7629.
40. Iwai, H., Nakajima, Y., Natori, S., Arata, Y., and Shimada, I. (1993) *Eur. J. Biochem. 217*, 639−644.
41. Yi, G. S., Park, C. B., Kim, S. C., and Cheong, C. (1996) *FEBS Lett. 398*, 87−90.
42. Rozek, T., Waugh, R. J., Steinborner, S. T., Bowie, J. H., Tyler, M. J., and Wallace, J. C. (1998) *J. Pept. Sci. 4*, 111−115.
43. Dempsey, C. E. (1990) *Biochim. Biophys. Acta 1031*, 143−161.
44. Bechinger, B. (1997) *J. Membr. Biol. 156*, 197−211.
45. Habermann, E. (1972) *Science 177*, 314−322.
46. Rex, S. (2000) *Biophys. Chem. 85*, 209−228.
47. Dempsey, C. E., Bazzo, R., Harvey, T. S., Syperek, I., Boheim, G., and Campbell, I. D. (1991) *FEBS Lett. 281*, 240−244.

BI035760B